

1 **Rhythmic interactions between the mediodorsal thalamus** 2 **and prefrontal cortex precede human visual perception**

3

4 Benjamin J. Griffiths¹, Tino Zaehle², Stefan Reppinger^{2,3}, Friedhelm C. Schmitt², Jürgen
5 Voges⁴, Simon Hanslmayr⁵, Tobias Staudigl^{1*}

6

7 Affiliations

8 1) Department of Psychology, Ludwig-Maximilians-Universität München, Munich, Germany

9 2) Department of Neurology, Otto-von Guericke-University, Magdeburg, Germany

10 3) ESF International Graduate School on Analysis, Imaging and Modelling of Neuronal and
11 Inflammatory Processes, Otto-von-Guericke University, Magdeburg, Germany

12 4) Department of Stereotactic Neurosurgery, Otto-von-Guericke University, Magdeburg, Germany

13 5) Centre for Cognitive Neuroimaging, Institute for Neuroscience and Psychology, University of
14 Glasgow, UK

15

16 * Corresponding Author:

17 Tobias Staudigl (tobias.staudigl@psy.lmu.de)

18 **Abstract**

19 The thalamus is much more than a simple sensory relay. High-order thalamic nuclei, such as
20 the mediodorsal thalamus, exert a profound influence over animal cognition. However, given
21 the difficulty of directly recording from the thalamus in humans, next-to-nothing is known about
22 thalamic and thalamocortical contributions to human cognition. To address this, we analysed
23 simultaneously-recorded thalamic iEEG and whole-head MEG in six patients (four female, two
24 male; plus MEG recordings from twelve healthy controls) as they completed a visual detection
25 task. We observed that the phase of both ongoing mediodorsal thalamic and prefrontal low-
26 frequency activity was predictive of perceptual performance. Critically however, mediodorsal
27 thalamic activity mediated prefrontal contributions to perceptual performance. These results
28 suggest that it is thalamocortical interactions, rather than cortical activity alone, that is predictive
29 of upcoming perceptual performance and, more generally, highlights the importance of
30 accounting for the thalamus when theorising about cortical contributions to human cognition.

31 **Introduction**

32 Thalamic contributions to cognition have been profoundly underestimated ¹. Contrary to a
33 cortico-centric view of cognition², a whole host of cognitive phenomena rely on the thalamus
34 and its interactions with the cortex ^{3,4}. For example, animal models suggest that it is the
35 interactions between the mediodorsal thalamus and the prefrontal cortex, as opposed to the
36 actions of the prefrontal cortex alone, that dictate the outcome of tasks that have traditionally
37 been thought of as “prefrontal-dependent” (e.g. attentional control; working memory ⁵⁻⁸). This
38 thalamic dependency is not surprising considering that the prefrontal cortex has literally been
39 defined as any frontal region that receives innervation from the mediodorsal thalamus ^{9,10}. As
40 such, an interaction between these two regions in service of cognition seems plausible, yet
41 evidence for such a phenomenon in humans is conspicuously absent.

42 It is a challenge to record human thalamic electrophysiological activity directly from the
43 source, and this challenge is compounded by the difficulty to record such activity simultaneously
44 with cortical activity. However, with access to simultaneous iEEG-MEG recordings, we can
45 begin to address the relevance of thalamocortical interactions to human cognition – in this case,
46 with a focus on visual detection. Within the cortex, visual detection has been linked to prefrontal
47 low-frequency activity (6-14Hz) ¹¹⁻¹⁶, but, as highlighted above, the prefrontal cortex doesn't act
48 in isolation. One could therefore postulate that these prefrontal low-frequency rhythms reflect
49 connections to mediodorsal thalamus through so-called thalamocortical loops ¹⁷⁻¹⁹. To
50 investigate this possibility, we analysed simultaneously-recorded intracranial
51 electroencephalography (iEEG; targeting the mediodorsal thalamic nuclei) and whole-brain
52 magnetoencephalography (MEG) in six patients (four female, two male) as they completed a
53 visual detection task (see figure 1a-b; see methods for commentary on sample size).
54 Additionally, we analysed MEG recordings in twelve healthy participants undergoing the same
55 task.

56 **Results**

57 In the first instance, we asked whether the phase of ongoing low-frequency activity in the
58 mediodorsal thalamus was predictive of visual detection. Morlet wavelets were used to extract
59 measures of instantaneous phase, and then the phase angles for “hits” (i.e., when the correct
60 stimulus was selected) and “misses” (i.e., when the incorrect stimulus was selected) were
61 contrasted using the phase bifurcation index (PBI) ¹¹. We expected to find a positive PBI, which

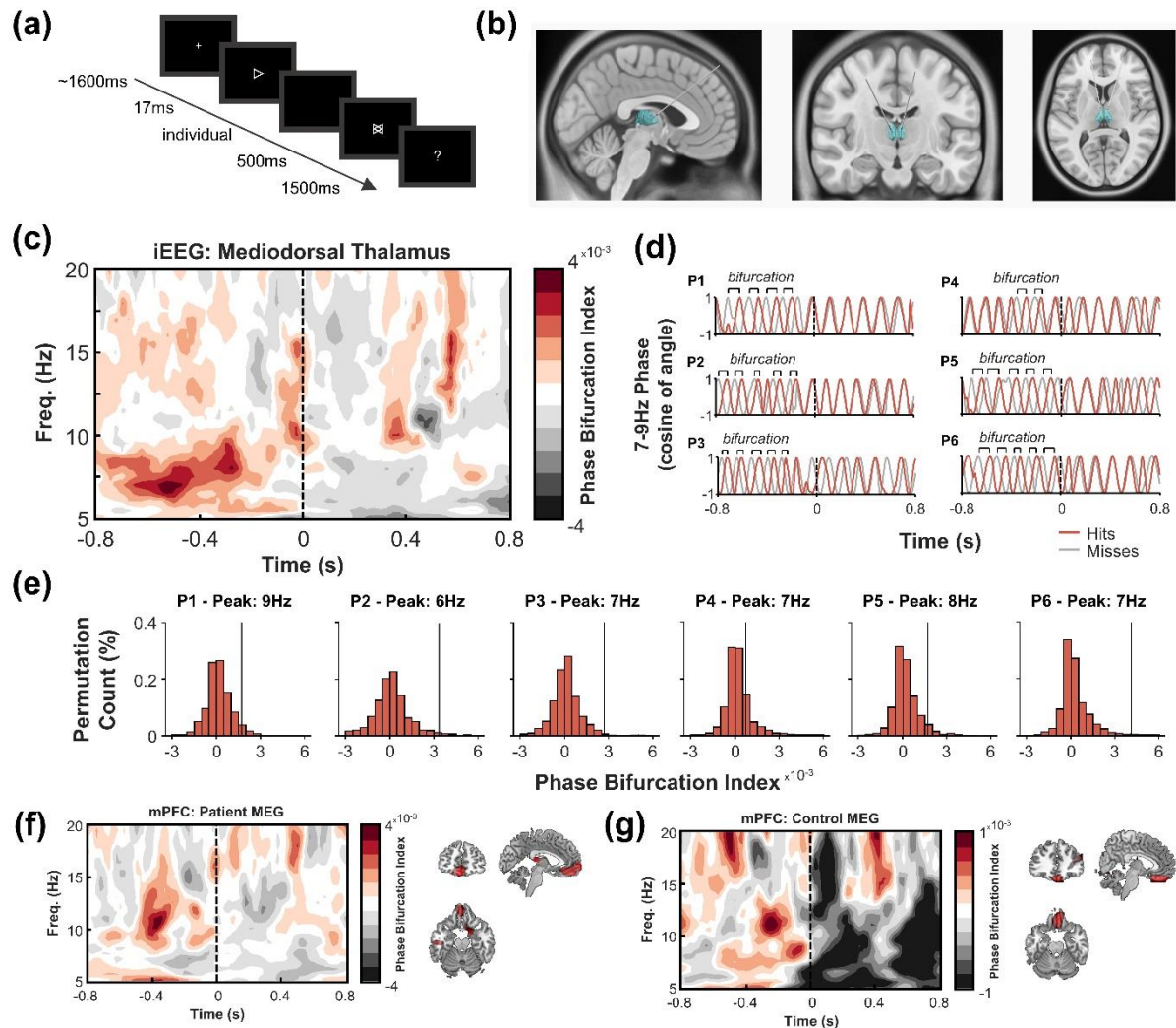


Figure 1. Phase bifurcation within the mediodorsal thalamus precedes visual detection. (a) Experiment overview. Participants completed a visual detection screen in which an arrow (pointed left or right) was briefly shown before a mask appeared. Participants then indicated which direction they thought the arrow was pointing. (b) Deep brain stimulation electrodes were implanted in the left and right mediodorsal and anterior thalami. See supplementary figure 1 for visualisation of mediodorsal thalamus in the context of other thalamic nuclei. (c) Time-frequency representation depicting mean mediodorsal thalamic phase bifurcation across patients (as measured with iEEG). Higher values indicate greater phase bifurcation. Time at 0s represents onset of the target. Substantial low-frequency phase bifurcation was observed prior to stimulus onset. (d) Bandpass-filtered (7-9Hz) mediodorsal thalamic signal for each participant individually (hits in red; misses in grey). The phases of the two conditions are opposed in all patients. (e) Patient-specific observed phase-bifurcation (black line) compared to a surrogate distribution (histogram) for individual peak bifurcation frequencies. The comparatively slow frequency effect of participant 2 did not impact the group effect (see supplementary figure 3). (f) MEG-recorded time-frequency representation (left) of medial prefrontal phase-bifurcation in patients and source-localisation of the peak of this effect (right; visualised phase bifurcation at -400ms, 10Hz; MNI: [-4, 50, -21]). (g) MEG-recorded time-frequency representation of medial prefrontal phase-bifurcation (left) in healthy controls and source-localisation of the peak of this effect (right; visualised phase bifurcation at -300ms, 11Hz; MNI: [5, 36, -24]). Figure abbreviations: iEEG – intracranial electroencephalography; MEG – magnetoencephalography; mPFC – medial prefrontal cortex

62 would indicate that there is a consistent phase angle difference between the two conditions prior
63 to stimulus onset.

64 Indeed, using this approach, we observed a positive PBI in the mediodorsal thalamus that
65 was significantly greater than what would be expected by chance (peaking at 7 to 8Hz, 600 to
66 300ms prior to stimulus onset; mean cluster $t(5) = 5.90$, $p_{clus} < 0.001$, Bayes Factor $[BF_{10}] =$

67 23.49; see figure 1c), indicating that there was an “optimal” mediodorsal thalamic phase for
68 visual detection. This could be observed in every participant (see figure 1d-e). No robust phase
69 bifurcation was observed in additional anterior thalamic recordings ($t(4) = 4.20$, $p_{clus} > 0.5$, BF_{10}
70 $= 5.63$; though no difference in PBI was observed between the anterior and mediodorsal
71 thalami: $t(5) = 7.52$, $p_{clus} = 0.094$, $BF_{10} = 25.84$; see supplementary figure 2).

72 Notably, the phase of the ongoing low frequency activity of several participants seemed to
73 undergo a rapid shift reminiscent of a phase reset following stimulus onset (see figure 1d). To
74 investigate this, we looked at how spectral power fluctuated as an interaction between time (pre-
75 stimulus vs. post-stimulus) and signal derivation technique (total power vs. evoked power).
76 Previous work²⁰ has suggested that an interaction in which evoked post-stimulus power
77 increases relative to pre-stimulus power, but total power does not, would indicate that the phase
78 of the signal has aligned across trials. However, we observed no such interaction ($F(1, 5) =$
79 1.04 , $p = 0.355$; see supplementary figure 5), suggesting that phase did not reorganise
80 consistently across participants following stimulus onset.

81 While several studies have linked low-frequency power to visual perception^{21–25}, we did
82 not observe any significant relationship between mediodorsal thalamic low-frequency power
83 and visual detection ($t(5) = 2.92$, $p_{clus} = 0.453$, $BF_{10} = 2.83$; see supplementary figure 4).

84 When shifting focus from the thalamus to the cortex, we found that similar pre-stimulus
85 phase patterns within the source-localised medial prefrontal cortex were predictive of upcoming
86 perceptual performance (mean cluster $t(5) = 10.62$, $p_{clus} = 0.016$, $BF_{10} = 198.21$; see figure 1f).
87 This effect was replicated in the healthy control sample (mean cluster $t(11) = 3.52$, $p_{clus} = 0.031$,
88 $BF_{10} = 10.76$; see figure 1g) with highly similar spatial localisation, and conforms to earlier
89 reports of the phase of low-frequency prefrontal oscillations predicting upcoming perceptual
90 performance^{11,12,15}. While there were minor differences in the timing and spectral profile of the
91 pre-stimulus effects in the patient and control samples, this was not significant (mean cluster
92 $t(16) = 3.15$, $p_{clus} = 0.662$; $BF_{10} = 7.71$). There was, however, a strong negative PBI following
93 stimulus onset for the healthy controls relative to the patient sample (mean cluster $t(16) = -6.44$,
94 $p_{clus} < 0.001$, $BF_{10} = 1558.32$; see figure 1f and 1g). This negative PBI seemed to be driven by
95 the evoked response to the stimulus (see supplementary figure 6). We were unable to ascertain
96 why the evoked response effect was restricted solely to the healthy controls, but given that this
97 effect is restricted solely to the post-stimulus window, and no post-stimulus effect could
98 retroactively alter a pre-stimulus effect, we feel that this open question does not undermine our
99 central results.

100 Previous studies have also observed phase bifurcation over the dorsal attention network
101 (e.g. ^{12,26}). While the positioning of the electrode wires during the patient MEG recording
102 prevents us from reliably probing these more posterior sources (see supplementary figure 7),
103 the healthy control MEG recordings show analogous results to those which have been reported
104 previously (see supplementary figure 8).

105 Given the presence of perceptually-relevant phase separation in both the mediodorsal
106 thalamus and the medial prefrontal cortex, we then asked whether these two regions connected
107 on a trial-by-trial basis. To this end, we used inter-site phase clustering (ISPC [i.e., phase-
108 locking value across sites²⁷, where a value of ‘0’ indicates no clustering and ‘1’ indicates
109 maximal phase clustering]) to quantify the pre-stimulus low-frequency phase consistency
110 between the mediodorsal thalamus and every voxel of the source-reconstructed MEG signal.
111 Across all trials, connectivity was greatest between the mediodorsal thalamus and the ipsilateral
112 medial prefrontal cortex, at approximately 8Hz, and was significantly greater than expected by

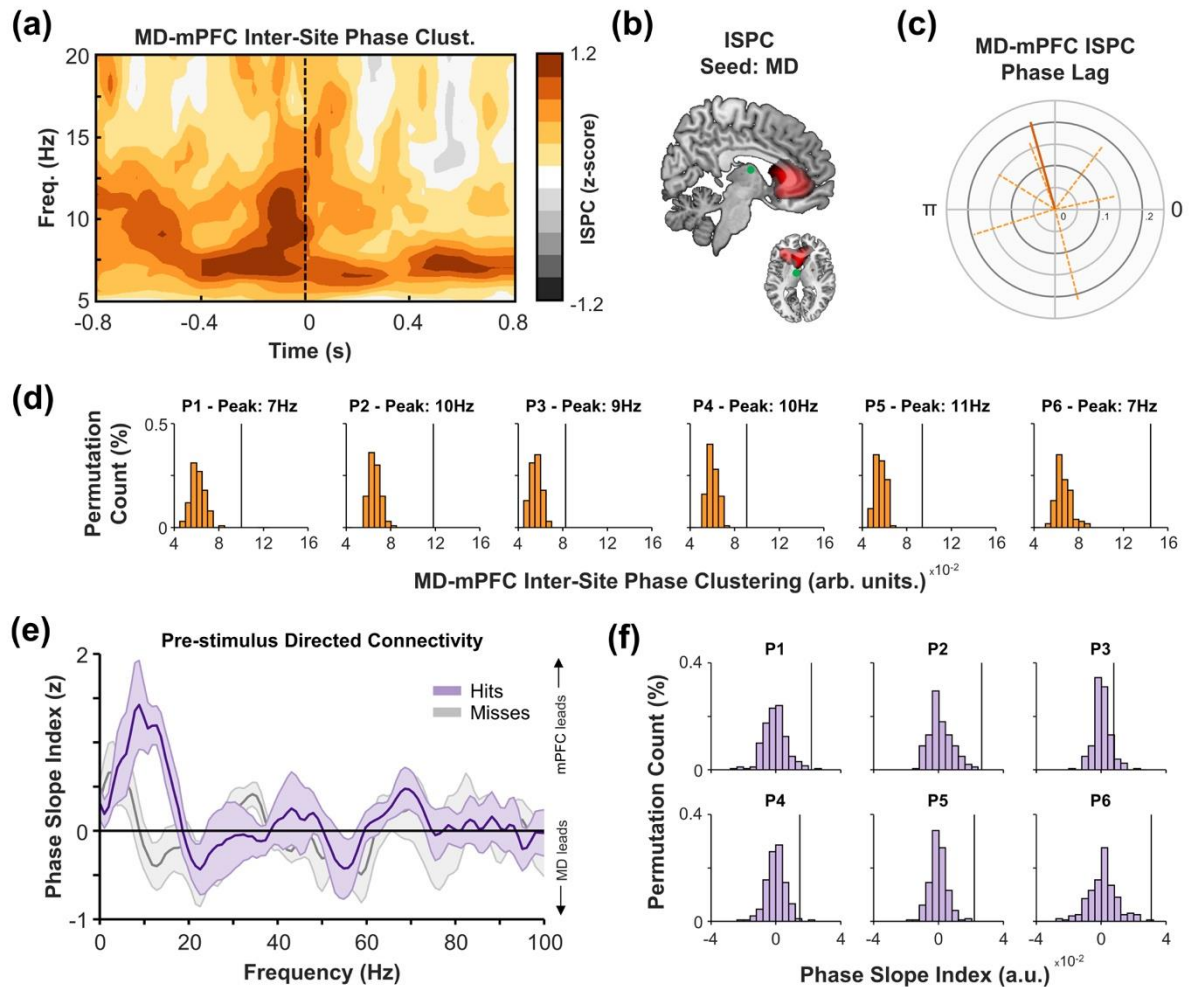


Figure 2. Corticothalamic connectivity precedes visual detection. (a) Time-frequency representation of phase-based undirected connectivity between intracranial recordings of the mediiodorsal thalamus and MEG recordings of the medial prefrontal cortex. Connectivity peaked prior to stimulus onset, at ~8Hz. (b) Pre-stimulus 8Hz phase-based undirected connectivity between the mediiodorsal thalamus and source-localised MEG signals peak in the ipsilateral prefrontal cortex (insert: left reflects ipsilateral hemisphere, right reflects contralateral). Green circle indicates approximate position of mediiodorsal thalamic electrode. (c) Polar plot of mean phase lag between mediiodorsal thalamus and medial prefrontal cortex. The dark, solid orange line indicates mean phase lag and mean vector length of the participant-specific phase lag angle; light, dotted orange lines indicate mean phase lag and mean vector length per participant). The scale ranges from zero (i.e., no consistent direction) to one (i.e., perfectly consistent lag across participants/trials). Note that the mean phase lag/vector length across participants was calculated only using the phase lags of the individual participants (that is, the calculation was not weighted by participant-specific mean vector length). (d) Patient-specific observed connectivity (black line) compared to surrogate distributions (orange histograms) for individual peak connectivity frequencies. (e) Frequency spectrum for pre-stimulus directed connectivity between medial prefrontal cortex and mediiodorsal thalamus (hits in purple, misses in grey). A positive value indicates that the medial prefrontal cortex leads the mediiodorsal thalamus, while a negative value indicates the mediiodorsal thalamus leads the medial prefrontal cortex. The medial prefrontal cortex leads the mediiodorsal thalamus uniquely for hits. (f) Patient-specific observed directed connectivity (black line) compared to surrogate distributions (purple histograms) individual peak directed connectivity frequencies. Figure abbreviations: ISPC – Inter-site phase clustering; MD – mediiodorsal thalamus; mPFC – medial prefrontal cortex.

113 chance (mean cluster $t(5) = 19.83$, $p_{clus} < 0.001$, $BF_{10} = 2,218.64$; see figure 2a-c; see
 114 supplementary figure 8). This effect was substantial in all patients (see figure 2d). A link between
 115 this corticothalamic connectivity and perceptual performance was inconclusive (mean cluster
 116 $t(5) = 5.37$, $p_{clus} = 0.188$, $BF_{10} = 17.13$; see supplementary figure 9).

117 When assessing the directionality of this connectivity using the Phase Slope Index (PSI)²⁸
 118 across all trials, the medial prefrontal cortex appeared to “lead” low-frequency activity in the
 119 mediodorsal thalamus to a significantly greater degree than chance (mean cluster $t(5) = 5.33$,
 120 $p_{\text{clus}} < 0.001$, $BF_{10} = 16.73$). This directed connectivity was predictive of perceptual performance,
 121 as prefrontal-to-thalamic PSI was greater for hits relative to misses (mean cluster $t(5) = 8.26$,
 122 $p_{\text{clus}} < 0.001$, $BF_{10} = 11.71$; see figure 2e-f).

123 Intriguingly, we also observed directed connectivity in which low-frequency activity in the
 124 mediodorsal thalamus preceded low-frequency activity posterior sources (mean cluster $t(5) = -$
 125 8.15 , $p_{\text{clus}} = 0.063$, $BF_{10} = 73.96$). Given that MEG coverage of these posterior sources was
 126 inconsistent across participants (see supplementary figure 7), we have decided to avoid resting
 127 any major conclusions based on these thalamus-to-posterior cortex connections. Nonetheless,
 128 the interested reader can turn to supplementary figure 10 for more details.

129 Lastly, we asked whether the mediodorsal thalamus mediates prefrontal contributions to
 130 visual detection. To this end, we developed a simple mediation model where prefrontal low-
 131 frequency activity could influence perceptual performance directly (see pathway c' in figure 3a)
 132 or indirectly (i.e., via the mediodorsal thalamus; see pathway ab in figure 3a). In this model, the
 133 indirect pathway predicted perceptual performance to a degree greater than what would be
 134 expected by chance ($t(5) = 3.85$, $p < 0.001$, $BF_{10} = 12.05$; see figure 3b for participant-specific
 135 plots of the observed magnitude for the indirect pathway relative to chance). Moreover, when
 136 contrasting the magnitude of pathway c (that is: the direct influence of pre-stimulus prefrontal
 137 cortical activity on behavioural performance without accounting for thalamic activity) against
 138 pathway c' (i.e., the direct influence of pre-stimulus prefrontal cortical activity on behavioural
 139 performance after accounting for thalamic activity), we found evidence to suggest that the direct
 140 influence of pre-stimulus prefrontal cortical activity on behavioural performance was diminished
 141 after accounting for pre-stimulus thalamic activity ($t(5) = 2.26$, $p = 0.031$, $BF_{10} = 3.06$). Similar
 142 results can be found when using partial correlations in place of a mediation model (see
 143 supplementary figure 11). This suggests that the mediodorsal thalamus mediates prefrontal
 144 activity to some degree. However, the direct effect of the medial prefrontal cortex on visual
 145 detection continued to explain the outcome to a significant degree after accounting for the

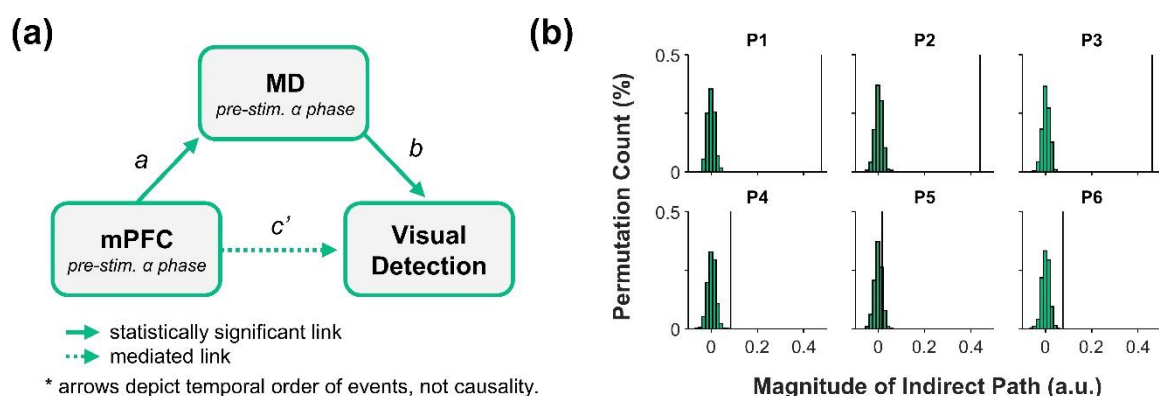


Figure 3. Mediodorsal thalamic phase bifurcation mediates prefrontal contributions to visual detection.
(a) Visualisation of the proposed mediation model. Pre-stimulus low-frequency phase patterns within the medial prefrontal cortex predict visual perceptual performance both directly and/or indirectly via the mediodorsal thalamus. Statistical analysis suggests that the indirect pathway (ab) better predicts behavioural performance than the direct pathway. **(b)** The predictive power of the observed indirect path (ab , black line) on behavioural performance relative to chance (histogram bars; 1,000 permutations). Figure abbreviations: MD – mediodorsal thalamus; mPFC – medial prefrontal cortex.

146 indirect effect ($t(5) = 32.99$, $p < 0.001$, $BF_{10} = 33,187.91$ [though this is a large Bayes Factor,
147 this is not surprising given the region of interest was selected by identifying the where and when
148 prefrontal rhythms best predicted visual detection prior to accounting for mediodorsal thalamic
149 activity; see methods for details]). This suggests that the prefrontal cortex is not completely
150 redundant in this visual detection task. Nonetheless, these results suggest that mediodorsal
151 thalamic phase bifurcation is not simply an epiphenomenon induced by phase-based
152 correlations with the prefrontal cortex. Rather, the mediodorsal thalamus appears to partially
153 mediate prefrontal contributions to visual perception.

154 Discussion

155 In sum, we find evidence to suggest that visual detection fluctuates as a function of pre-
156 stimulus, low-frequency mediodorsal thalamic phase; a phenomenon which mirrors cortical
157 patterns that have been reported previously (e.g. ¹¹⁻¹³). Moreover, we find that directed coupling
158 between the cortex and thalamus, in which prefrontal activity leads mediodorsal thalamic activity
159 prior to stimulus onset. Critically however, it appears that the mediodorsal thalamus mediates
160 these cortical contributions to visual detection performance (see figure 4 for visual summary of
161 the main results).

162 Of course, a key question remains: what do corticothalamic interactions contribute to visual
163 detection? A recent framework ²⁹ suggests that the thalamus acts as a “Bayesian observer”, in
164 which high-order thalamic nuclei use sensory input to update “templates” of the environment
165 maintained in the cortex ^{30,31}. Based upon this, one could speculate that the mediodorsal
166 thalamus helps contrast existing cortical templates (maintained in the prefrontal cortex ^{5,32,33})
167 with current sensory input. When a mismatch arises between the current input and the prefrontal
168 representation, the mediodorsal thalamus
169 updates this template (e.g., by down-
170 weighting the past representation and
171 stabilising the new representation ³⁴), which
172 is then acted upon ³⁵. Notably,
173 computational models suggest that these
174 mechanistic interactions produce patterns of
175 low-frequency travelling waves between the
176 interacting regions³⁶, which may explain why
177 corticothalamic connectivity was most
178 prevalent in the low frequencies. If template
179 updating were to breakdown, one could
180 expect that the detection of a transient
181 change in sensory input would fail and
182 corticothalamic low-frequency connectivity
183 would dissipate, which may explain why the
184 directional connectivity from the prefrontal
185 cortex to the mediodorsal thalamus
186 observed here was performance-
187 dependent. While the correlative nature of
188 our data prevents us testing these ideas,
189 future studies which disrupt corticothalamic
190 interactions (e.g., through direct thalamic

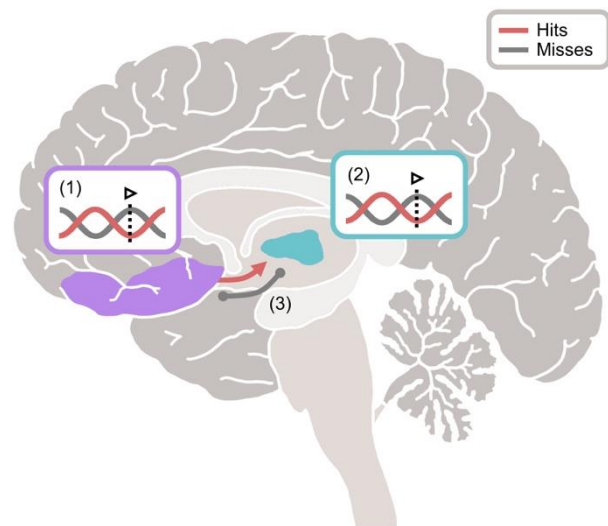


Figure 4. Visual depiction of the main findings. Successful detection of a visual stimulus correlates with several neural phenomena: (1) the stimulus being presented at the optimal, low-frequency phase of ongoing medial prefrontal activity (mPFC in purple; hits in red; misses in grey), (2) the stimulus being presented at the optimal, low-frequency phase of ongoing mediodorsal thalamic activity (mediodorsal thalamus in aqua; hits in red; misses in purple), and (3) directed prefrontal-to-thalamic low-frequency connectivity (hits in red; misses [which displayed undirected connectivity] in grey). Critically, the contribution of the prefrontal cortex to visual detection appears to be mediated by the mediodorsal thalamus.

191 stimulation) could directly test the causal nature of these hypotheses.

192 An alternative explanation of the rhythmic corticothalamic interaction stems from works
193 investigating interactions between the pulvinar and cortical attentional networks. Directional
194 interactions between the cortical attentional network and the pulvinar (another high-order
195 thalamic nucleus) rhythmically fluctuate at a rate similar to that which we observe here ^{37,38}.
196 Functionally speaking, this phase-based switching is thought to correspond to switching
197 between cognitive tasks: namely, sampling the environment and shifting attention ³⁹. Perhaps a
198 similar phenomenon arises between the prefrontal cortex and mediodorsal thalamus: one phase
199 of the oscillation favours the transfer of sensory/maintained representations to the mediodorsal
200 thalamus, while the other phase supports the updating of the cortical template. This would
201 translate to rhythmic fluctuations in perceptual performance, where stimuli presented during the
202 phase optimal for cortex-to-thalamus communication are more likely to be perceived than those
203 presented during the phase optimal for thalamus-to-cortex communication (which matches with
204 our observation that cortex-to-thalamus directed connectivity is predictive perceptual
205 performance). Again, future studies may turn to methods such as brain stimulation to directly
206 test the causal nature of this hypothesis.

207 One may be wondering why prefrontal cortical and mediodorsal thalamic phase bifurcation
208 arose at neighbouring, rather than identical, frequencies (~11Hz and ~8Hz respectively). While
209 the spectral smearing incurred through the use of wavelets for our measure of inter-site phase
210 clustering and the 6Hz bandwidth used for the phase-slope index analyses provide a
211 mathematical explanation of connectivity between the two differing frequency bands, it wouldn't
212 explain the physiological underpinnings of such a phenomenon. We speculate, however, that
213 the observed connectivity in conjunction with the mild difference in frequency may relate to
214 travelling waves (e.g. ^{40,41}); more specifically, travelling waves that come about through weakly-
215 coupled oscillators⁴². Models of weakly-coupled oscillators suggest that travelling waves can
216 couple two regions so long as the oscillator of the transmitting region has a higher intrinsic
217 frequency than the oscillator of the receiving region. In the case of the data presented here, we
218 would anticipate that a travelling wave would begin within the prefrontal cortex (given its higher
219 peak phase bifurcation frequency) and propagate to the mediodorsal thalamus. Notably, such
220 an idea neatly ties to the phase-slope index results which demonstrated directed connectivity
221 from the prefrontal cortex to the mediodorsal thalamus. Moreover, this explanation also aligns
222 with the "Bayesian observer" described above, and the travelling waves inherent in such a
223 hypothesis³⁶. Of course, this remains a speculative interpretation of the frequency differences
224 between the two regions as very little is known about corticothalamic travelling waves in
225 humans. Consequently, such an explanation presents a novel avenue for future research
226 regarding corticothalamic interactions, and may provide an answer as to why two regions with
227 differing bifurcating frequencies may relate to a shared phenomenon.

228 Our observation of low-frequency connectivity between the mediodorsal thalamus and
229 prefrontal cortex suggests that humans exhibit similar thalamocortical loops to those observed
230 in animals ^{18,38}. To date, studies of these loops in humans are scarce ⁴³, owing to the fact that
231 simultaneous, direct recordings of the specific thalamic nuclei and cortex are rare (see ⁴⁴⁻⁴⁷ for
232 other examples recording from various thalamic nuclei). As such, to understand these moment-
233 by-moment dynamics, the field has had to rely on generalising earlier findings from animal
234 models to humans, rather than studying humans directly. While these models have provided
235 fantastic advances in our understanding of the role of the thalamocortical loops in visual
236 perception, they do have their limitations. Firstly, many of these studies have focused on the
237 pulvinar (e.g., ^{37,38}), whose anatomical and functional connections to the cortex are notably

238 different to the cortical connections of the mediodorsal thalamus, meaning these results cannot
239 be generalised to explain the role of the mediodorsal thalamus in visual perception. Second,
240 animal models of the prefrontal cortex are limited in their generalisability relative to animal
241 models of other cortical regions owing to the unique evolutionary divergence in structure of the
242 prefrontal cortex⁴⁸, meaning prefrontal-thalamic connections in humans remain poorly
243 understood. The data we present here helps overcome these hurdles and demonstrate how
244 synchronised low-frequency activity facilitates interactions between the human cortex and
245 thalamus.

246 While numerous studies have suggested that prefrontal activity predicts^{11–16}, and perhaps
247 causes^{49–52}, fluctuations in perceptual performance, evidence is far from consistent^{21,53–56}.
248 Perhaps this is due to overlooking the role of the mediodorsal thalamus and its many
249 connections to the prefrontal cortex. Indeed, given that we found evidence to suggest that the
250 mediodorsal thalamus mediates prefrontal contributions to visual perception, this may explain
251 why cortico-centric investigations of the neural correlates of visual perception produce such
252 inconsistent results.

253 Beyond the prefrontal cortex, numerous other cortical regions have been shown to engage
254 in visual perceptual processes (e.g., the dorsal attention network;^{12,26}). Due to the positioning
255 of the iEEG wires in the MEG, however, we were unable to reliably record signals from these
256 regions, and hence investigate how they interact with the mediodorsal thalamus. Despite this
257 however, we observed interesting connectivity dynamics where low-frequency thalamic activity
258 seemingly leads low-frequency activity in the occipital cortex (see supplementary figure 10). In
259 the context of the prefrontal connectivity patterns, one could speculate that signals from the
260 prefrontal cortex pass to the occipital lobe via the mediodorsal thalamus, and may explain why
261 phase opposition effects can be seen across the cortex^{e.g.11,12,26}. Of course, given that these
262 results depend on signals generated from sources with poor MEG sensor coverage, one must
263 take these findings with a grain of salt.

264 Going forth, our findings emphasise the importance of accounting for the thalamus when
265 probing prefrontal contributions to human cognition^{1,29,57}, and, more generally, highlight the
266 importance of shifting from a cortico-centric model of human cognition towards a more
267 integrative, thalamocortical model.

268 **Methods**

269 *Participants*

270 We recruited six patients (66.6% female, mean age: 41.2 ± 8.9 years, 100% right-handed) with
271 bilateral intracranial depth electrodes implanted in the anterior nuclei of the thalamus for deep brain
272 stimulation therapy of drug-resistant epilepsy for the experiment. We recorded electrophysiological
273 signals from these intracranial electrodes simultaneously with those from an MEG system (see acquisition
274 details overleaf). The measurements were approved by the Ethics Commission of the Medical Faculty of
275 the Otto-von-Guericke University, Magdeburg.

276 A sample size of six for an experiment such as this is small (see <https://osf.io/tyfwu/> for a constantly-
277 updating table on similar experiments; mean size: 14.8 participants; std: 6.3), though to be expected
278 given the rarity of (i) patients being treated with deep brain stimulation of the thalamus, (ii) access to
279 thalamic electrophysiology in these patients (DBS leads are externalized only in a minority of these
280 patients post-surgery, allowing the present combination of intracranial thalamic recordings and cognitive
281 experiments), and (iii) the summation of the rarity of intracranial recordings and the rarity of the possibility
282 to simultaneously acquire MEG recordings. The problems with such samples are twofold: a heightened

283 likelihood of a false positive, and a heightened likelihood of a false negative. The heightened likelihood
284 of a false positive can, in part, be attributed to the group mean being more easily swayed by a single
285 outlier. To attenuate such a concern here, we have visualised participant-specific effects (see figures 1e,
286 2d, 2h, 3b) to demonstrate that the effect is not driven by a single participant, but is instead a consistent
287 trend across patients. The heightened likelihood of a false negative can be attributed to a lack of statistical
288 power. To attenuate this concern, we have supplemented the null-hypothesis testing procedure with a
289 report of Bayes Factor (i.e., the strength of evidence for the alternative, relative to null, hypothesis). While
290 Bayesian analyses are not impervious to issues of low statistical power⁵⁸, they can provide a better
291 indication as to whether the absence of an effect is attributable to a genuine null effect, or insufficient
292 power. As a heuristic, a Bayes Factor of less than 3 is considered “anecdotal evidence” for H_1 relative to
293 H_0 , a Bayes Factor between 3 and 10 is considered “moderate evidence” for H_1 relative to H_0 , and a
294 Bayes Factor greater than 10 can be considered “strong evidence” for H_1 relative to H_0 .

295 We recruited an additional 12 healthy controls (50% female, mean age = 27.6 ± 6.5 years, 100%
296 right-handed), who did not suffer epilepsy and therefore had no intracranial electrodes, to complete the
297 same task while undergoing MEG. Handedness was assessed using the Edinburgh Handedness
298 Inventory. *[https://doi.org/10.1016/0028-3932\(71\)90067-4](https://doi.org/10.1016/0028-3932(71)90067-4).

299 *Paradigm*

300 Figure 1a illustrates the experimental procedure. Before the start of the experiment, each participant
301 completed a staircase procedure (2-up-1 down) varying the duration of the blank interval after the stimulus
302 to maintain a detection rate of ~71% correct trials in the actual experiment. For the experiment,
303 participants were instructed to focus their attention on the centre of the screen in order to discriminate
304 the direction of an arrow (left or right). They completed several practice trials to familiarize themselves
305 with the procedure. Prior to the target stimulus, a fixation cross with a uniformly variable duration (1500-
306 1700ms) was presented. Following this, the target (an arrow pointing either to the left or the right) was
307 presented for 1 frame (corresponding to 16.7ms [60 Hz refresh rate] for the patients and 8.3 ms [120 Hz
308 refresh rate] for the healthy participant sample). After the arrow, a blank screen was presented. The
309 duration of the blank screen was determined by the staircase procedure described above. At the lower
310 end of the staircase (less than 1 frame), the blank screen was omitted. Following the blank screen, a
311 mask consisting of an overlay of both arrows appeared for 500ms. This mask ensures that the brain
312 perceives the stimulus for the same amount of time across trials, as the presentation of said mask
313 minimises retinal after-effects and post-stimulus visual processing⁵⁹. Subsequently, a question mark
314 prompted the participants to indicate the direction of the arrow by pressing one of two designated
315 response buttons. The participants were instructed beforehand to always give a response, and in case of
316 uncertainty, to guess. The participants were also instructed to respond as fast as possible. The response
317 window lasted for 1500ms, limiting the time window for each response. Every participant completed 6
318 blocks, each of which consisted of 72 trials. Participants were given the opportunity for a short break in
319 between each block.

320 For patients, the mean hit rate across participants was 75.9% (s.d. 14.7%), and the mean reaction
321 time was 872ms (s.d. 203ms). For the healthy controls, the mean hit rate across participants was 80.3%
322 (s.d. 10.3%), and the mean reaction time was 750ms (s.d. 78ms).

323 *iEEG acquisition*

324 The two thalamic depth electrodes each had four intracranial electrode contacts (platinum–iridium
325 contacts, 1.5 mm wide with 1.5 mm edge-to-edge distance). The clinically-relevant implantation target
326 was the anterior thalamic nucleus. However, due its small size and the implantation trajectory, a subset
327 of the electrode contacts invariably land in the mediodorsal thalamus (see Fig. 1b). All patients received
328 bilateral implants, resulting in eight electrode contacts in the thalamic area. iEEG was recorded by feeding
329 the signal into auxiliary channels of the MEG system, ensuring simultaneous recordings and synchronized
330 triggers across iEEG and MEG. All recordings were continuously sampled at 678.17 Hz.

331 *iEEG electrode localisation*

332 We estimated the locations of these contacts using the Lead-DBS software⁶⁰. First, we co-registered
333 the post-operative CT scan to pre-operative T1-weighted image using a two-stage linear registration (rigid
334 followed by affine) as implemented in Advanced Normalisation Tools⁶¹. Second, we spatially normalised
335 these scans to MNI space based on the pre-operative T1-weighted image using the Unified Segmentation
336 Approach as implemented in SPM12⁶². Third, we reconstructed the positions and trajectories of the DBS
337 electrodes based on post-operative CT scan. Fourth, we corrected these reconstructions for brainshift in
338 post-operative acquisitions by applying a refined affine transform calculated between pre- and post-
339 operative scans that were restricted to a subcortical area of interest (as implemented in the Lead-DBS
340 software). Lastly, we visually confirmed the positions of the contacts using the DISTAL Atlas⁶³. Full details
341 of electrode positioning can be found in supplementary table 1. All analyses were performed separately
342 on mediodorsal thalamic pairs, or anterior thalamic pairs.

343 *iEEG preprocessing*

344 The iEEG recordings underwent several steps to attenuate artifacts. All preprocessing steps were
345 completed using the Fieldtrip toolbox⁶⁴. First, we downsampled the iEEG recordings to 500Hz. Second,
346 we filtered the recordings using a 150Hz Butterworth low-pass filter (order = 6), two Butterworth band-
347 stop filters (to attenuate line noise; 49-51Hz, 99-101Hz; order = 6), and a 0.5Hz Butterworth high-pass
348 filter (order = 6). Third, we epoched the recordings around the onset of the visual target, starting 2 seconds
349 before target onset and ending 2 seconds after target onset. Fourth, we inspected the recordings for
350 artifactual/epileptic activity, and any trials or channels exhibiting such activity were excluded (percentage
351 of electrodes removed: 33.3% [+/- 21.1%]; percentage of trials removed: 15.6% [+/- 6.7%]).

352 *iEEG re-referencing*

353 Following artifact rejection, we re-referenced the iEEG recordings using a bipolar re-referencing
354 montage to provide a measure of spatially-specific activity within the anterior and mediodorsal thalamic
355 nuclei. All six patients had at least one bipolar-referenced electrode pair within the mediodorsal thalamus,
356 and five of these patients had at least one bipolar-referenced electrode pair within the anterior thalamus.
357 We first identified all bipolar pairs that would feasibly capture mediodorsal/anterior thalamic activity of a
358 given participant, and then selected the pair which produced the cleanest mediodorsal/anterior thalamic
359 evoked response (see supplementary figure 12 for evoked response of the selected pairs). As we used
360 post-stimulus evoked activity as our selection criteria, and our main analyses focused on the pre-stimulus
361 window, we can assume that this selection procedure did not introduce issues of circularity into our main
362 analyses⁶⁵. Full details of bipolar electrode positioning and pairing can be found in Supplementary Table
363 1.

364 *Patient MEG acquisition and preprocessing*

365 We recorded MEG with a 248-channel whole-cortex magnetometer (MAGNES 3600, 4D
366 Neuroimaging, San Diego, USA) in a magnetically shielded room. Patients sat upright in the MEG. All
367 recordings were continuously sampled at 678.17 Hz. MEG data of patients 1,2 and 3 were DC recorded,
368 MEG data of patients 4, 5 and 6 was recorded with a bandwidth of 0.1-200 Hz. We digitised the patients'
369 nasion, left and right ear canal, and head shape prior to each session with a Polhemus 3Space Fasttrack.

370 The recordings underwent several steps to attenuate artifacts. All preprocessing steps were
371 completed using the Fieldtrip toolbox⁶⁴. First, we downsampled the MEG recordings to 500Hz. Second,
372 we filtered the recordings using a 150Hz Butterworth low-pass filter (order = 6), two Butterworth band-
373 stop filters (to attenuate line noise; 49-51Hz, 99-101Hz; order = 6), and a 5Hz Butterworth high-pass filter
374 (order = 6). This high-pass filter was set at 5Hz as slower-frequency activity (i.e., <5Hz) was corrupted
375 by movement-related artifacts introduced by the presence of iEEG recording equipment within the dewar
376 (note: to address concerns that the phase bifurcation effect in the medial prefrontal cortex was artifactually
377 driven by this filter, we also analysed an independent set of MEG data from healthy participants where a
378 less aggressive filter was used [0.5Hz; see below]). Third, we epoched the recordings around the onset

379 of the visual target, starting 2 seconds before target onset and ending 2 seconds after target onset.
380 Fourth, we denoised the MEG recordings by conducting PCA on reference channels (as implemented in
381 the Fieldtrip function `ft_denoise_pca`). Fifth, we used ICA to detect and remove spatially-stationary
382 artifacts including eye blinks, eye movements, cardiac artifacts, and residual motion related artifacts.
383 Sixth, we inspected the recordings for artifactual/epileptic activity. Any trials/sensors exhibiting such
384 activity were excluded (percentage of sensors removed: 38.6% [+/- 7.1%]; percentage of trials removed:
385 45.0% [+/- 10.8%]; see next paragraph for notes of these high percentages). Lastly, we reconstructed the
386 preprocessed data in source space using individual head models and structural (T1-weighted) MRI scans.
387 We reconstructed the time-locked MEG data using a single-shell forward model and a Linearly
388 Constrained Minimum Variance beamformer (LCMV; ⁶⁶), with the lambda regularisation parameter set to
389 5%.

390 It is important to note that the externalised wires of the intracranial electrodes introduced substantial
391 noise into the MEG recordings, with many posterior MEG sensors becoming saturated as a result of
392 noise. Across patients, few sensors remained over parietal and occipital regions (see supplementary
393 figure 7 for a topographic plot of artifactual sensors). We therefore refrain from drawing major conclusions
394 based upon results observed in posterior sources.

395 *Healthy control MEG acquisition and preprocessing*

396 For the healthy control subjects, we recorded MEG with a 306-channel whole-cortex magnetometer
397 (Elekta Neuromag TRIUX, Elekta, Stockholm, Sweden) in a magnetically shielded room. Participants sat
398 upright in the MEG. All recordings were sampled at 2,000Hz and online-filtered with a pass-band of 0.1-
399 660Hz. Headshape was digitized analogue to patient's measurements.

400 As above, we downsampled the MEG recordings to 500Hz. Second, we filtered the recordings using
401 a 165Hz Butterworth low-pass filter (order = 6), two Butterworth band-stop filters (to attenuate line noise;
402 49-51Hz, 99-101Hz; order = 6), and a 0.5Hz Butterworth high-pass filter (order = 6). Third, we epoched
403 the recordings around the onset of the visual target, starting 2 seconds before target onset and ending 2
404 seconds after target onset. Fourth, we used ICA to detect and remove spatially-stationary artifacts
405 including eye blinks, eye movements, cardiac artifacts, and residual motion related artifacts. Fifth, we
406 inspected the recordings for artifactual activity. Any trials/channels exhibiting such activity were excluded.
407 LCMV beamforming was conducted in the same manner as described above.

408 *Phase bifurcation analyses*

409 All subsequent analyses were conducted using a combination of in-house custom code (available
410 here: <https://github.com/StaudiglLab/corticothalamic-connect>) and the Fieldtrip toolbox. In instances
411 where we relied on custom code, the key equations are given. In instances where we used prebuilt
412 Fieldtrip functions, those functions are explicitly named.

413 In the first instance, we asked whether the phase of pre-stimulus low-frequency band activity within
414 the mediodorsal thalamus predicts visual detection. First, we estimated the phase of the pre-processed
415 mediodorsal thalamic recordings using 6-cycle wavelets (33 linearly spaced estimates ranging from -
416 800ms to 800ms [that is, sampled every 50ms]; for frequencies ranging from 5 to 20Hz [in steps of 1Hz])
417 Note that we expanded beyond the pre-stimulus window for the purpose of data visualisation (e.g., see
418 fig 1c). Second, we split trials into two conditions based on whether the response on said trial was correct
419 (from here on termed "hits") or incorrect (from here on termed "misses"). Third, we computed the phase
420 bifurcation index (PBI) as described by Busch and colleagues (2009). Here, inter-trial phase clustering
421 [ITPC; also termed 'phase locking value' (PLV); see eq. (1)] for each condition was computed separately
422 (ITPC_{hits} and ITPC_{misses}), as well as inter-trial phase clustering for both conditions combined (ITPC_{combined}).
423 The ITPC values were then used to estimate phase bifurcation [see eq. (2)].

424
$$ITPC = \left| n^{-1} \sum_{r=1}^n e^{ik_r} \right| \quad (eq.1)$$

425 where: n = number of trials, and k = phase angle

426
$$PBI = (ITPC_{hits} - ITPC_{combined}) * (ITPC_{misses} - ITPC_{combined}) \quad (eq.2)$$

427 It is worth noting that this measure suffers a trial number bias: conditions with fewer trials see higher
428 scores than conditions with more trials. To address this, we created a shuffled baseline in which every
429 trial was circularly shifted in time (preserving signal autocorrelation) by a random number of samples and
430 the phase bifurcation index was recalculated using this shuffled data (1,000 permutations). This shuffled
431 baseline retained the trial imbalance present in the initial calculation, and retained the phase structure of
432 every trial, but should no longer exhibit any phase clustering beyond what would be expected by chance.
433 We then z-transformed the PBI derived from the real data using the mean and standard deviation of the
434 permutations of the shuffled baseline to give an estimate of phase bifurcation relative to chance.

435 For statistical analysis, we pooled together the z-transformed PBI of each patient and conducted a
436 group-level, cluster-based, permutation test⁶⁷ (using 64 permutations; i.e., every possible permutation
437 from a sample of six patients [2⁶]). To aid in the interpretability of the cluster (that is, one cannot state
438 exact when a “significant” cluster arises, only that has arisen in the time-frequency window analysed; see
439⁶⁸), we restricted the cluster analysis to the pre-stimulus period (i.e., -800ms to stimulus onset) and to the
440 frequency range where this effect has been observed in previous studies of the cortex (i.e., 6-14Hz; see
441⁶⁹ for meta-analysis). Cluster analysis addressed issues of multiple comparisons across time and
442 frequency while the spectrotemporal region of interest ensured spectral/temporal specificity to pre-
443 stimulus low-frequencies. As we only used a single mediodorsal thalamic channel (derived from a bipolar-
444 referenced electrode pair) from each participant for this analysis, there were no multiple comparisons
445 across space.

446 To supplement the main statistical result, we report the Bayes Factor at the peak voxel. Bayes factor
447 was computed using the *bayesFactor* toolbox (<https://github.com/klabhub/bayesFactor>). We selected a
448 default prior for the Bayesian t-test (i.e., the Cauchy prior $[2/\sqrt{2}]$)⁷⁰.

449 To address the issue of the wavelet-induced smearing of a post-stimulus effect into the pre-stimulus
450 window, we repeated the statistical analysis as above, but with the exclusion of any pre-stimulus sample
451 point where the edges of the wavelet (for a given frequency) would extend into the post-stimulus window.
452 After excluding the pre-stimulus time bins that could be compromised by wavelet-induced temporal
453 smearing of a post-stimulus effect, phase bifurcation continued to be observed (mean cluster $t(5) = 2.65$,
454 $p_{clus} = 0.047$, $BF_{10} = 22.25$).

455 We repeated the entirety of this analytical pipeline for the anterior thalamic recordings.

456 We then applied this same approach to the source-reconstructed MEG data. As before, the z-
457 transformed phase bifurcation index for each participant was pooled and subjected to a group-level,
458 cluster-based, permutation test (this time using the Fieldtrip function *ft_sourcestatistics*). When
459 statistically appraising phase bifurcation in the patient MEG data ($n=6$), 64 permutations were used once
460 again. As the function *ft_sourcestatistics* cannot conduct cluster analyses across time/frequency while
461 simultaneously conducting analyses across space, we averaged the PBI values across the pre-stimulus
462 window (i.e., -800ms to stimulus onset) and across the frequency range where this effect has been
463 observed in previous studies of the cortex (i.e., 6-14Hz; see⁶⁹ for meta-analysis), which provided a single
464 PBI value for each voxel of source-reconstructed MEG data. The cluster analysis was then conducted
465 across space on this time/frequency averaged data. We repeated the process for the healthy control MEG
466 ($n=12$), however, 4096 permutations were used (i.e., 2¹² permutations) in place of 64 permutations.

467 *Phase reset analysis*

468 To test whether the phase of ongoing activity resets following stimulus onset, we computed low-
469 frequency spectral power (6 to 9Hz; in steps of 1Hz) across the epoch (-800ms to 800; in steps of 25ms)
470 using 6-cycle wavelets, and then took the average ‘pre-stimulus’ power just before stimulus onset (-200
471 to 0ms) and ‘post-stimulus’ power just after stimulus onset. We conducted this spectral decomposition

472 twice: first, on single trials before averaging the result across trials (i.e., total power), and second, on the
473 trial-averaged amplitude (i.e., evoked power). If phase does reset after stimulus onset, then phase should
474 align across trials after stimulus onset, and will present as an increase in evoked power for post-stimulus
475 activity relative to pre-stimulus activity. In contrast, no change in total power will be observed on the single
476 trial level. To statistically appraise the effect, we conducted a 2x2 repeated measures ANOVA to probe
477 how spectral power changed as a function of epoch (pre- vs. post-stimulus) and decomposition method
478 (single trial decomposition vs. trial-averaged decomposition).

479 Note that while phase clustering metrics are also sensitive to phase resets, they are not specific
480 (that is, a spike in phase clustering after stimulus onset may reflect a phase reset, but may also reflect
481 an evoked response). In contrast, the approach used here can be both sensitive and specific to phase
482 resets, as the evoked response component would be consistent across the total- and evoked power
483 metrics.

484 *Inter-site phase clustering connectivity analyses*

485 To assess whether the mediodorsal thalamus couples with the cortex prior to visual perception, we
486 examined inter-site phase clustering (ISPC) between the thalamic recordings and the source-
487 reconstructed MEG recordings. First, we estimated oscillatory phase using wavelets (no parameters were
488 changed from the phase bifurcation analyses described above). Second, we computed the circular
489 distance between the instantaneous phase angle in the thalamus and the phase angle in the source-
490 reconstructed voxel (individually for every trial, timepoint, frequency and source-reconstructed voxel). We
491 then computed ISPC clustering over trials [see eq. (3); note that this is identical to eq. (1), with the
492 exception that it uses the phase angle difference between two regions, rather than a single, observed
493 phase angle].

494
$$ISPC = \left| n^{-1} \sum_{r=1}^n e^{id_r} \right| \quad (eq. 3)$$

495 where: n = number of trials, and d = circular distance between phase angles

496 To examine whether the observed ISPC differed from chance, we generated a distribution of chance
497 ISPC values by randomly shuffling the trials of the thalamus recordings relative to the MEG recordings
498 and re-computing the ISPC (total permutations = 1,000). We then z-transformed the observed ISPC using
499 the mean and standard deviation of the chance distribution (as done for the PBI measure). Statistical
500 analysis matched that of the PBI analyses on the source-reconstructed MEG signal (that is: cluster-based
501 permutation tests with a specific focus on pre-stimulus low-frequency activity).

502 To evaluate whether this connectivity varied as a function of perceptual performance, we calculated
503 ISPC for hits and misses separately, with a subsampling procedure used for hits to ensure trial numbers
504 were balanced across the two conditions. We then directly contrasted the resulting ISPCs in a cluster-
505 based permutation test (again, across voxels using *ft_sourcestatistics*, with each voxel matching the value
506 of the average of low-frequency [6-14Hz], pre-stimulus [-800 to 0ms] ISPC for that voxel).

507 It is worth noting that the ISPC can be biased by volume conduction. In such instances, the phase
508 lag between the thalamus and source-reconstructed MEG should cluster heavily around 0 or 180
509 degrees. This was not the case in our data (see figure 2c). Residual concerns about spurious
510 corticothalamic coupling are addressed by our “phase slope index” analysis below, which excludes zero-
511 lag angle differences from the computation.

512 *Phase slope index analyses*

513 To assess the directionality of the coupling between the mediodorsal thalamus and cortex, we used
514 the phase slope index²⁸. To this end, we calculated the Fourier spectrum of the pre-stimulus signal (-800
515 to 0ms) using a Hanning tapered FFT approach, and used the resulting signal to compute the PSI (as

516 implemented by the function *ft_connectivity_psi* in the Fieldtrip toolbox). As before, we compared the
517 observed PSI to chance by shuffling the trials of the thalamus recordings relative to the MEG recordings
518 and re-computing the PSI (total permutations = 200 [the number of permutations were reduced relative
519 to the analyses above due to computational limitations]). We then z-transformed the observed PSI using
520 the mean and standard deviation of the chance distribution (as done for the PBI and ISPC measures).
521 Statistical analysis matched that of the PBI and ISPC analyses on the source-reconstructed MEG signal.

522 We repeated this approach for hits and misses separately. The resulting z-transformed PSI
523 measures were directly compared in a group-level, cluster-based, permutation test.

524 *Mediation analyses*

525 To assess the possible mediating effect of the mediodorsal thalamus, we first set out to measure
526 phase bifurcation on the single-trial level. As the phase bifurcation index relies on data from all trials, such
527 an approach cannot be used to create trial-level models of mediation. Instead, for a given patient, and for
528 every pre-stimulus sample point, we took the mean phase angle across all “hit” trials, and then derived
529 the mean resultant vector between this “hit-averaged” phase angle and the observed angle on a given
530 trial (“hits” and “misses”). This provides a value between 0 and 1 which indicates how close the given trial
531 was to the “optimal” phase for subsequent visual detection [the higher the value, the closer the phase]²².

532 We then used a series of patient-specific regression models to assess (1) whether the distance to
533 the optimal phase within the medial prefrontal cortex predicts visual detection (independently of the
534 mediodorsal thalamus) [see eq. 4], (2) whether the distance to the optimal phase within the medial
535 prefrontal cortex predicts the distance to the optimal phase within the mediodorsal thalamus [see eq. 5],
536 and (3) whether the distance to the optimal phase within both the mediodorsal thalamus and the medial
537 prefrontal cortex, in combination, predicts visual detection [see eq. 6].

$$538 \quad Y = j_1 + cX \quad (\text{eq. 4})$$

$$539 \quad M = j_2 + aX \quad (\text{eq. 5})$$

$$540 \quad Y = j_3 + c'X + bM \quad (\text{eq. 6})$$

541 Where Y represents perceptual outcome (either hit or miss), X represents distance to optimal phase
542 in the medial prefrontal cortex, M represents distance to optimal phase in the mediodorsal thalamus, and
543 j represents the intercepts. When predicting Y, logistic models were used. When predicting M, linear
544 models were used. As the scaling of coefficients differs between these two models, all coefficients were
545 standardised by dividing by the standard error of fit. This brought both forms of coefficients into the same
546 unit space.

547 While, in theory, one can test this at every time, frequency and source-reconstructed voxel, this is
548 prohibitively computationally expensive (~14 days on our hardware). In addition, it is debatable as to
549 whether any meaningful measure of mediation can be derived from moments (be that timepoints,
550 frequencies or voxels) where the independent or mediator variable does not reliably predict the dependent
551 variable⁷¹. Therefore, for the sake of computational efficiency and statistical validity, we restricted our
552 analyses to the moments in which phase bifurcation peaked in the medial prefrontal cortex and
553 mediodorsal thalamus. While such an approach would inflate the likelihood of finding a link between
554 physiology and behaviour, given that the purpose of this analysis is to compare the relative link of the
555 mediodorsal thalamus and prefrontal cortex to behaviour (as opposed to the absolute link to behaviour),
556 we do not believe that this is a concern.

557 In our first test for mediation, we assessed whether the indirect effect (i.e., the *ab* pathway in figure
558 3a) differed significantly from zero. The indirect pathway describes the extent to which mediodorsal
559 thalamic phase bifurcation explains the impact of medial prefrontal cortical phase bifurcation on
560 perceptual performance. Thus, if this is significantly greater than zero, one can conclude that the influence
561 of the medial prefrontal cortex on perceptual performance is mediated by the mediodorsal thalamus in
562 some way, shape or form. To this end, we operationalised the indirect effect as the product of t-statistics
563 of a and b, normalised by the variance (see eq. 7, taken from ⁷²).

564

$$ab = \frac{t_a t_b}{\sqrt{t_a^2 + t_b^2 + 1}} \text{ (eq. 7)}$$

565 Where t_a and t_b are the standardised coefficients derived from eq. 5 and eq. 6 respectively. We then
566 z-transformed the magnitude of this effect using the mean and standard deviation of “chance-level”
567 indirect effects (which were calculated by shuffling the trials of the mediodorsal thalamic recordings
568 relative to the behavioural and medial prefrontal measurements and recomputing the regression models;
569 1,000 permutations). We then pooled the z-transformed measure of the indirect effect of each patient and
570 contrasted them against the null hypothesis that the indirect effect was no greater than chance (i.e., $z =$
571 0) in a permutation-based t-test. Here, for each permutation, the sign of each patient’s z-transformed
572 indirect effect was randomly assigned, and the t-values were recomputed. The p-value was then derived
573 by comparing the “true” t-value to this surrogate distribution.

574 In our second test of mediation, we asked whether the influence of medial prefrontal activity on
575 perceptual performance is diminished after accounting for mediodorsal thalamic activity. To this end, we
576 contrasted the “total effect” (c in eq. 4) against the “direct effect” (c' in eq. 6). If the direct effect is
577 significantly smaller than the total effect, one can infer that the second regressor in eq. 6 (i.e., the distance
578 to the optimal phase in the mediodorsal thalamus) has a mediating influence over prefrontal contributions
579 to visual detection. As above, we z-transformed the observed difference between the total and direct
580 effects using the mean and standard deviation of “chance-level” differences (which were calculated by
581 shuffling the trials of the medial prefrontal and mediodorsal thalamic recordings relative to the behavioural
582 data and recomputing the regression models; 1,000 permutations). We then pooled the z-transformed
583 difference of each patient and contrasted them against the null hypothesis that there was no difference
584 between the total and direct effects (i.e., $z = 0$) in a permutation-based t-test.

585 We supplemented the mediation analysis with an approach based on partial correlations (see
586 supplementary figure 11). We computed the single trial measures of distance to the optimal phase as
587 above, but rather than using logistic models to assess the relationship between brain activity and
588 perceptual performance, we used correlations and partial correlations. Specifically, we computed a
589 Spearman’s Rank correlation between the distance to the optimal medial prefrontal low-frequency phase
590 and perceptual performance, and a partial Spearman’s Rank correlation between the distance to the
591 optimal medial prefrontal low-frequency phase and perceptual performance while accounting for the
592 distance to the optimal mediodorsal thalamic low-frequency phase.

593 Note that, while mathematically plausible, inverting the mediation model such that the mediodorsal
594 thalamus becomes the independent variable and the medial prefrontal cortex becomes the purported
595 mediator would be conceptually invalid as our PSI analyses have demonstrated that the cortex precedes
596 the thalamus, and mediation analyses rest upon the assumption that the mediator follows the independent
597 variable in time⁷³. In other words, event A cannot mediate the influence of event B on event C if neither
598 event B nor C have happened yet.

599 **Acknowledgments**

600 We are indebted to all patients who volunteered their time to participate in this study.

601

602 **Author contributions:**

603 Conceptualization: TZ, SH, TS; Resources: TZ, FCS, JV; Investigation: TZ, SR, TS; Formal Analysis:
604 BJJ, TS; Funding acquisition: SH, TS; Project administration: TZ; Writing – original draft: BJJ, TS; Writing
605 – review & editing: BJJ, TZ, SR, FCS, JV, SH, TS.

606

607 **Competing interests:**

608 The authors declare no competing interests.

609

610 **Funding:**

611 European Research Council, Starting Grant 802681 (TS), Consolidator Grant 647954 (SH), Economic
612 Social Sciences Research Council ES/R010072/1 (SH).

613

614 **Data availability:**

615 The associated data is available upon reasonable request.

616

617 **Code availability:**

618 The code used for this study is available at: <https://github.com/StaudiglLab/corticothalamic-connect>.

619

620 **References**

- 621 1. Sherman, S. M. The thalamus is more than just a relay. *Curr. Opin. Neurobiol.* **17**, 417–422 (2007).
- 622 2. Parvizi, J. Corticocentric myopia: old bias in new cognitive sciences. *Trends Cogn. Sci.* **13**, 354–359
623 (2009).
- 624 3. Acsády, L. The thalamic paradox. *Nat. Neurosci.* **20**, 901–902 (2017).
- 625 4. Halassa, M. M. & Kastner, S. Thalamic functions in distributed cognitive control. *Nat. Neurosci.* **20**,
626 1669–1679 (2017).
- 627 5. Bolkan, S. S. *et al.* Thalamic projections sustain prefrontal activity during working memory
628 maintenance. *Nat. Neurosci.* **20**, 987–996 (2017).
- 629 6. Schmitt, L. I. *et al.* Thalamic amplification of cortical connectivity sustains attentional control. *Nature*
630 **545**, 219–223 (2017).
- 631 7. Guo, Z. V. *et al.* Maintenance of persistent activity in a frontal thalamocortical loop. *Nature* **545**, 181–
632 186 (2017).
- 633 8. Parnaudeau, S. *et al.* Inhibition of Mediodorsal Thalamus Disrupts Thalamofrontal Connectivity and
634 Cognition. *Neuron* **77**, 1151–1162 (2013).
- 635 9. Rose, J. E. & Woolsey, C. N. The orbitofrontal cortex and its connections with the mediodorsal
636 nucleus in rabbit, sheep and cat. *Res. Publ. Assoc. Res. Nerv. Ment. Dis.* **27**, 210–210 (1948).
- 637 10. Carlén, M. What constitutes the prefrontal cortex? *Science* **358**, 478–482 (2017).
- 638 11. Busch, N. A., Dubois, J. & VanRullen, R. The phase of ongoing EEG oscillations predicts visual
639 perception. *J. Neurosci.* **29**, 7869–7876 (2009).
- 640 12. Zazio, A., Ruhnau, P., Weisz, N. & Wutz, A. Pre-stimulus alpha-band power and phase fluctuations
641 originate from different neural sources and exert distinct impact on stimulus-evoked responses. *Eur.*
642 *J. Neurosci.* [ejn.15138](https://doi.org/10.1111/ejn.15138) (2021) doi:10.1111/ejn.15138.
- 643 13. Dugué, L., Marque, P. & VanRullen, R. The phase of ongoing oscillations mediates the causal relation
644 between brain excitation and visual perception. *J. Neurosci.* **31**, 11889–11893 (2011).
- 645 14. Fiebelkorn, I. C. *et al.* Cortical cross-frequency coupling predicts perceptual outcomes. *NeuroImage*
646 **69**, 126–137 (2013).
- 647 15. Manasseh, G. *et al.* Retinal and post-retinal contributions to the quantum efficiency of the human eye
648 revealed by electrical neuroimaging. *Front. Psychol.* **13** (2013).
- 649 16. Fakche, C., VanRullen, R., Marque, P. & Dugué, L. Alpha phase-amplitude tradeoffs predict visual
650 perception. *bioRxiv* 1–29 (2021).
- 651 17. Berger, H. The human electroencephalogram. *Nat. Sci.* **23**, 121–124 (1935).

- 652 18. Lopes da Silva, F. H., van Lierop, T. H. M. T., Schrijer, C. F. & Storm van Leeuwen, W. Organization
653 of thalamic and cortical alpha rhythms: Spectra and coherences. *Electroencephalogr. Clin.*
654 *Neurophysiol.* **35**, 627–639 (1973).
- 655 19. Hughes, S. W. & Crunelli, V. Thalamic Mechanisms of EEG Alpha Rhythms and Their Pathological
656 Implications. *The Neuroscientist* **11**, 357–372 (2005).
- 657 20. Jutras, M. J., Fries, P. & Buffalo, E. A. Oscillatory activity in the monkey hippocampus during visual
658 exploration and memory formation. *Proc. Natl. Acad. Sci.* **110**, 13144–13149 (2013).
- 659 21. Benwell, C. S. Y., Coldea, A., Harvey, M. & Thut, G. Low pre-stimulus EEG alpha power amplifies
660 visual awareness but not visual sensitivity. *Eur. J. Neurosci.* ejn.15166 (2021)
661 doi:10.1111/ejn.15166.
- 662 22. Hanslmayr, S. *et al.* Prestimulus oscillations predict visual perception performance between and
663 within subjects. *NeuroImage* **37**, 1465–1473 (2007).
- 664 23. Samaha, J., Iemi, L., Haegens, S. & Busch, N. A. Spontaneous brain oscillations and perceptual
665 decision-making. *Trends Cogn. Sci.* 1–15 (2020) doi:10.1016/j.tics.2020.05.004.
- 666 24. Samaha, J., Iemi, L. & Postle, B. R. Prestimulus alpha-band power biases visual discrimination
667 confidence, but not accuracy. *Conscious. Cogn.* **54**, 47–55 (2017).
- 668 25. Griffiths, B. J. *et al.* Alpha/beta power decreases track the fidelity of stimulus-specific information.
669 *eLife* **8**, 1–22 (2019).
- 670 26. Mathewson, K. E., Gratton, G., Fabiani, M., Beck, D. M. & Ro, T. To see or not to see: Prestimulus
671 α phase predicts visual awareness. *J. Neurosci.* **29**, 2725–2732 (2009).
- 672 27. Lachaux, J. P., Rodriguez, E., Martinerie, J. & Varela, F. J. Measuring phase synchrony in brain
673 signals. *Hum. Brain Mapp.* **8**, 194–208 (1999).
- 674 28. Nolte, G. *et al.* Robustly Estimating the Flow Direction of Information in Complex Physical Systems.
675 *Phys. Rev. Lett.* **4** (2008).
- 676 29. Rikhye, R. V., Wimmer, R. D. & Halassa, M. M. Toward an Integrative Theory of Thalamic Function.
677 *Annu. Rev. Neurosci.* **41**, 163–183 (2018).
- 678 30. Wicker, E., Turchi, J., Malkova, L. & Forcelli, P. A. Mediodorsal thalamus is required for discrete
679 phases of goal-directed behavior in macaques. *eLife* **7**, e37325 (2018).
- 680 31. Alcaraz, F. *et al.* Thalamocortical and corticothalamic pathways differentially contribute to goal-
681 directed behaviors in the rat. *eLife* **7**, e32517 (2018).
- 682 32. Rowe, J. B., Toni, I., Josephs, O., Frackowiak, R. S. J. & Passingham, R. E. The Prefrontal Cortex:
683 Response Selection or Maintenance Within Working Memory? *Science* **288**, 1656–1660 (2000).
- 684 33. Miller, E. K. & Cohen, J. D. An Integrative Theory of Prefrontal Cortex Function. *Annu. Rev. Neurosci.*
685 **24**, 167–202 (2001).
- 686 34. Rikhye, R. V., Gilra, A. & Halassa, M. M. Thalamic regulation of switching between cortical
687 representations enables cognitive flexibility. *Nat. Neurosci.* **21**, 1753–1763 (2018).
- 688 35. Watanabe, Y. & Funahashi, S. Thalamic mediodorsal nucleus and working memory. *Neurosci.*
689 *Biobehav. Rev.* **36**, 134–142 (2012).
- 690 36. Alamia, A. & VanRullen, R. Alpha oscillations and traveling waves: Signatures of predictive coding?
691 *PLOS Biol.* **17**, e3000487 (2019).
- 692 37. Fiebelkorn, I. C., Pinsk, M. A. & Kastner, S. The mediodorsal pulvinar coordinates the macaque
693 fronto-parietal network during rhythmic spatial attention. *Nat. Commun.* **10**, (2019).

- 694 38. Saalman, Y. B., Pinsk, M. A., Wang, L., Li, X. & Kastner, S. The pulvinar regulates information
695 transmission between cortical areas based on attention demands. *Science* **337**, 753–756 (2012).
- 696 39. Fiebelkorn, I. C. & Kastner, S. A rhythmic theory of attention. *Trends Cogn. Sci.* **23**, 87–101 (2019).
- 697 40. Zhang, H., Watrous, A. J., Patel, A. & Jacobs, J. Theta and Alpha Oscillations Are Traveling Waves
698 in the Human Neocortex. *Neuron* 1–13 (2018) doi:10.1016/j.neuron.2018.05.019.
- 699 41. Muller, L., Chavane, F., Reynolds, J. & Sejnowski, T. J. Cortical travelling waves: mechanisms and
700 computational principles. *Nat. Rev. Neurosci.* **19**, 255–268 (2018).
- 701 42. Ermentrout, G. B. & Kopell, N. Frequency Plateaus in a Chain of Weakly Coupled Oscillators, I. *SIAM*
702 *J. Math. Anal.* **15**, 215–237 (1984).
- 703 43. Halgren, M. *et al.* The generation and propagation of the human alpha rhythm. *Proc. Natl. Acad. Sci.*
704 *U. S. A.* **116**, 23772–23782 (2019).
- 705 44. Sarnthein, J. & Jeanmonod, D. High Thalamocortical Theta Coherence in Patients with Parkinson’s
706 Disease. *J. Neurosci.* **27**, 124–131 (2007).
- 707 45. Sarnthein, J. & Jeanmonod, D. High thalamocortical theta coherence in patients with neurogenic
708 pain. *NeuroImage* **39**, 1910–1917 (2008).
- 709 46. Staudigl, T. *et al.* Memory signals from the thalamus: Early thalamocortical phase synchronization
710 entrains gamma oscillations during long-term memory retrieval. *Neuropsychologia* **50**, 3519–3527
711 (2012).
- 712 47. Sweeney-Reed, C. M. *et al.* Pre-stimulus thalamic theta power predicts human memory formation.
713 *NeuroImage* **138**, 100–108 (2016).
- 714 48. Passingham, R. How good is the macaque monkey model of the human brain? *Curr. Opin. Neurobiol.*
715 **19**, 6–11 (2009).
- 716 49. Ciaramelli, E., Leo, F., Del Viva, M. M., Burr, D. C. & Ladavas, E. The contribution of prefrontal cortex
717 to global perception. *Exp. Brain Res.* **181**, 427–434 (2007).
- 718 50. Del Cul, A., Dehaene, S., Reyes, P., Bravo, E. & Slachevsky, A. Causal role of prefrontal cortex in
719 the threshold for access to consciousness. *Brain* **132**, 2531–2540 (2009).
- 720 51. Colás, I. *et al.* Conscious perception in patients with prefrontal damage. *Neuropsychologia* **129**, 284–
721 293 (2019).
- 722 52. Barceló, F., Suwazono, S. & Knight, R. T. Prefrontal modulation of visual processing in humans. *Nat.*
723 *Neurosci.* **3**, 399–403 (2000).
- 724 53. Ruzzoli, M., Torralba, M., Morís Fernández, L. & Soto-Faraco, S. The relevance of alpha phase in
725 human perception. *Cortex* **120**, 249–268 (2019).
- 726 54. Bompas, A., Sumner, P., Muthumaraswamy, S. D., Singh, K. D. & Gilchrist, I. The contribution of
727 pre-stimulus neural oscillatory activity to spontaneous response time variability. *NeuroImage* **12**
728 (2015).
- 729 55. Odegaard, B., Knight, R. T. & Lau, H. Should a few null findings falsify prefrontal theories of conscious
730 perception? *J. Neurosci.* **37**, 9593–9602 (2017).
- 731 56. Boly, X. M. *et al.* Are the neural correlates of consciousness in the front or in the back of the cerebral
732 cortex? Clinical and neuroimaging evidence. *J. Neurosci.* **11** (2017).
- 733 57. Kosciessa, J. Q., Lindenberger, U. & Garrett, D. D. Thalamocortical excitability modulation guides
734 human perception under uncertainty. *Nat. Commun.* **12**, 2430 (2021).
- 735 58. McNeish, D. On Using Bayesian Methods to Address Small Sample Problems. *Struct. Equ. Model.*
736 **23**, 750–773 (2016).

- 737 59. Enns, J. T. & Di Lollo, V. What's new in visual masking? *Trends Cogn. Sci.* **4**, 345–352 (2000).
- 738 60. Horn, A. & Kühn, A. A. Lead-DBS: A toolbox for deep brain stimulation electrode localizations and
739 visualizations. *NeuroImage* **107**, 127–135 (2015).
- 740 61. Avants, B. B., Epstein, C. L., Grossman, M. & Gee, J. C. Symmetric diffeomorphic image registration
741 with cross-correlation: Evaluating automated labeling of elderly and neurodegenerative brain. *Med.*
742 *Image Anal.* **12**, 26–41 (2008).
- 743 62. Ashburner, J. & Friston, K. J. Unified segmentation. *NeuroImage* **26**, 839–851 (2005).
- 744 63. Ewert, S. *et al.* Toward defining deep brain stimulation targets in MNI space: A subcortical atlas
745 based on multimodal MRI, histology and structural connectivity. *NeuroImage* **170**, 271–282 (2018).
- 746 64. Oostenveld, R., Fries, P., Maris, E. & Schoffelen, J.-M. FieldTrip: Open source software for advanced
747 analysis of MEG, EEG, and invasive electrophysiological data. *Comput. Intell. Neurosci.* **2011**, 1–9
748 (2011).
- 749 65. Kriegeskorte, N., Simmons, W. K., Bellgowan, P. S. F. & Baker, C. I. Circular analysis in systems
750 neuroscience: the dangers of double dipping. *Nat. Neurosci.* **12**, 535–540 (2009).
- 751 66. van Veen, B., van Drongelen, W., Yuchtman, M. & Suzuki, A. Localization of brain electrical activity
752 via linearly constrained minimum variance spatial filtering. *IEEE Trans. Biomed. Eng.* **44**, 867–880
753 (1997).
- 754 67. Maris, E. & Oostenveld, R. Nonparametric statistical testing of EEG- and MEG-data. *J. Neurosci.*
755 *Methods* **164**, 177–90 (2007).
- 756 68. Sassenhagen, J. & Draschkow, D. Cluster-based permutation tests of MEG/EEG data do not
757 establish significance of effect latency or location. *Psychophysiology* **56**, e13335 (2019).
- 758 69. VanRullen, R. Perceptual cycles. *Trends Cogn. Sci.* **20**, 723–735 (2016).
- 759 70. van Doorn, J. *et al.* The JASP Guidelines for Conducting and Reporting a Bayesian Analysis.
760 *psyArxiv* 38 (2020).
- 761 71. MacKinnon, D. P. & Fairchild, A. J. Current directions in mediation analysis. *Curr. Dir. Psychol. Sci.*
762 **18**, 16–20 (2009).
- 763 72. Iacobucci, D. Mediation analysis and categorical variables: The final frontier. *J. Consum. Psychol.* **13**
764 (2012).
- 765 73. MacKinnon, D. P., Fairchild, A. J. & Fritz, M. S. Mediation analysis. *Annu. Rev. Psychol.* **58**, 593–
766 614 (2007).
- 767